Journal of Materials Chemistry A

Accepted Manuscript

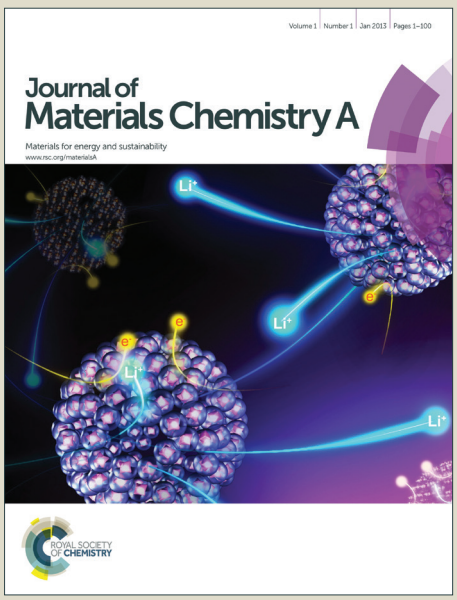

ROYAL SOCIETY OF CHEMISTRY

www.rsc.org/materialsA

Insights into Chirality Distributions of Single-Walled Carbon Nanotube Grown on Different $Co_xMg_{1-x}O$ Solid Solutions

Maoshuai He[1], Hua Jiang[2], Inkeri Kauppi[1], Pavel V. Fedotov[3], Alexander I. Chernov[3], Elena D. Obraztsova[3], Filippo Cavalca[4], Jakob B. Wagner[4], Thomas W. Hansen[4], Jani Sainio[2], Emma Sairanen[1], Juha Lehtonen[1], Esko I. Kauppinen[2]*

[1] Department of Biotechnology and Chemical Technology, Aalto University School of Chemical Technology, P.O. Box 16100, FI-00076 Aalto, Finland

[2] Department of Applied Physics, Aalto University School of Science, P.O. Box 15100, FI-00076 Aalto, Finland

[3] A.M. Prokhorov General Physics Institute RAS, 38 Vavilov Street, 119991 Moscow, Russia

[4] Center for Electron Nanoscopy, Technical University of Denmark, DK-2800 Kongens Lyngby, Denmark

Corresponding Author

* Correspondence should be addressed to: Maoshuai He, Email: hemaoshuai@gmail.com; Tel:+358 50 371 9188

Abstract:

Low-temperature chemical vapor deposition (CVD) growth of single-walled carbon nanotubes (SWNTs) was achieved on two different types of $Co_xMg_{1-x}O$ catalysts prepared by different techniques: atomic layer deposition (ALD) and impregnation. The chirality distribution of SWNTs grown on ALD-prepared $Co_xMg_{1-x}O$ is wider than that of SWNTs grown on the impregnation-prepared $Co_xMg_{1-x}O$ catalyst. The different chirality distributions of SWNTs are related to their different growth modes. The ALD-prepared $Co_xMg_{1-x}O$ catalyzes the growth of SWNTs by "tip growth" mode, as revealed by *in situ* environmental transmission electron microscopy studies. In contrast, SWNTs grow on the impregnation-prepared $Co_xMg_{1-x}O$ by "base growth" mode. The "base growth" is attributed to strong metal-support interactions between the epitaxially formed Co nanoparticles and the underlying MgO support, accounting for the synthesis of SWNTs with high chiral-selectivity. In addition, impregnation-prepared $Co_xMg_{1-x}O$ catalysts calcinated at different temperatures were systematically studied and their catalytic performances in synthesizing carbon nanotubes were elucidated. The work illustrates the influences of metal-support interactions and catalyst reducibility on the chirality-distribution of synthesized SWNTs.

Keywords: Single-walled carbon nanotube, epitaxial relationship, chiral-selective, solid solution, *in situ* environmental transmission electron microscopy

1. Introduction

A solid solution is defined as a solid phase where the crystal structure of the solvent remains unchanged by the addition of a solute. To form a solid solution, the solvent and the solute should have similar crystal structure and atomic radii. For example, face-centered cubic (*fcc*) MgO (lattice constant: 4.21 Å) has almost the same lattice parameter as *fcc* CoO (lattice constant: 4.26 Å), therefore, the two oxides can form a $Co_xMg_{1-x}O$ phase in which the ratio between the components can vary.[1-2] Metal

nanoparticles extracted by reducing the solid solution are stabilized by the underlying MgO support[1-3] and applicable for a variety of catalytic reactions, such as methane conversion to syngas[1] and carbon nanotube growth.[2-5] In these catalytic reactions, MgO is selected as the catalyst support because of not only its low cost and high thermal stability, but also its strong basicity which inhibits excessive carbon deposition and prolongs the lifetime of catalyst.[6] Furthermore, MgO can also be readily removed from carbon nanotubes by a mild acid treatment after growth,[6-8] rendering MgO-based solid solution an ideal catalyst for large-scale synthesis of carbon nanotubes.

Progress has been made in the past decade to develop transition metal oxide-MgO solid solutions for efficiently growing multi-walled,[2-3] double-walled,[7] or single-walled carbon nanotubes (SWNTs).[5] Building from the pioneering work by Chen *et al.*[3] on multi-walled carbon nanotube (MWNT) growth over a $Ni_xMg_{1-x}O$ solid solution, Flahaut et al. advanced a combusion-prepared $Co_{0.1}Mg_{0.9}O$ solid solution to grow SWNTs[5] or double-walled carbon nanotubes.[7] Carbon nanotubes grow on metal nanoparticles formed upon reducing the solid solutions. However, the high temperature required for solid solution reduction could cause severe aggregation of small metal particles, leading to the growth of carbon nanotubes with wide diameter distributions.[5] Consequently, solid solution catalyst with low reduction temperature is highly preferred for growing SWNTs with a narrow diameter (or even chirality) distribution.

Just recently, we have reported an impregnation-prepared $Co_xMg_{1-x}O$ solid solution for growing SWNTs with a high chirality selectivity for (6,5) tube.[4] An optimal calcination process for preparing the $Co_xMg_{1-x}O$ solid solution is to anneal a mixture of MgO and $Co(NO_3)_2$ at 1000 ^oC for 20 h. Upon reduction, uniform metallic Co nanoparticles form epitaxially on the catalyst surface, initiating the growth of SWNTs with a "base growth" mode.[4, 9] Despite progress in chiral-selective growth of SWNTs, the correlation between the SWNT chirality distribution and the growth mode remains a

relatively uncharted territory due to few catalysts capable of growing SWNTs with narrow chirality distributions. Similarly, the study of the MgO-supported-catalyst reducibility influence on the SWNT chirality distribution has been sparse. In order to extend our understandings of the characteristics of the catalyst that might influence the SWNT growth result, different $Co_xMg_{1-x}O$ catalysts need to be designed and systematic studies on SWNTs grown on them are required.

In this work, a series of $Co_xMg_{1-x}O$ solid solutions is prepared and applied for low temperature CVD growth of SWNTs. First, a $Co_xMg_{1-x}O$ solid solution prepared by ALD is exploited for growing SWNTs. The chirality distribution of the SWNTs is compared with that of SWNTs grown on the impregnation-prepared $Co_xMg_{1-x}O$ solid solution. Secondly, the SWNT growth mechanisms on ALD prepared $Co_xMg_{1-x}O$ are investigated by *in situ* environmental transmission electron microscopy (ETEM) studies and the reasons for different chirality-distributions of SWNTs grown on different $Co_xMg_{1-x}O$ solid solutions are elucidated. Finally, the influences of the reducibility on the catalytic performances of impregnation-prepared $Co_xMg_{1-x}O$ solid solutions are presented and discussed.

2. Materials and methods

2.1. Preparation of $Co_xMg_{1-x}O$ catalyst by ALD

The MgO support was obtained by thermal decomposition of magnesium carbonate hydroxide hydrate (Aldrich, 99%) at 400 °C for 1 h.[10-12] The catalyst preparation process was similar to that for preparing other supported Co catalysts.[13-15] Briefly, the Co deposition was carried out in an F120 reactor at a pressure of ~10 kPa. Cobalt (III) acetylacetonate (98%, Aldrich) was chosen as the metal precursor and the deposition temperature was set at 190 ^oC. After 6 h deposition, the catalyst was annealed at 450 ^oC with air to remove the acetylacetonate-ligands. The catalyst is denoted as ALD-$Co_xMg_{1-x}O$.

2.2. Preparation of $Co_xMg_{1-x}O$ catalysts by impregnation

The $Co_xMg_{1-x}O$ catalysts were prepared by impregnation of 4.0 g MgO with a aqueous solution of $Co(NO_3)_2$ (1.40 g $Co(NO_3)_2 \cdot 6H_2O$ in 100 mL H_2O, the atomic ratio between Co and Mg is about 5%). After drying in air, the mixtures were heated for 20 h at different temperatures. The prepared catalysts are denoted as $Co_xMg_{1-x}O$ (T), where T denotes the calcination temperature.

2.3. Characterizations of catalysts by X-ray diffraction (XRD) spectroscopy, X-ray photoelectron spectroscopy (XPS) and hydrogen temperature programmed reduction (H_2-TPR)

Information on the crystal structure of the catalysts was ascertained by XRD performed using an X'pert diffractmeter with Cu Kα at λ = 1.54 Å. XRD patterns were recorded over a range of *2θ* angles from 10^o to 90^o. XPS measurements were performed with a Surface Science SSX-100 ESCA spectrometer and an electrostatic hemispherical analyzer. Peak positions were calibrated using the O1s photoelectron peak of MgO at 530.5 eV as reference.[16]

H_2-TPR experiments were carried out in an Altamira AMI-100 characterization system equipped with mass spectrometer (Pfeiffer MS, Omnistar GSD 320) to analyze the gaseous products. Prior to H_2-TPR experiments, the catalysts were treated *in situ* under flowing 50 cm^3 of O_2/He gas mixture (10 vol % O_2 in He, AGA) and heated to 450 °C (ramp rate 10 °C/min) in order to remove impurities (carbonaceous species and water from the atmosphere) from the catalyst surface. H_2-TPR experiments were performed using a mixture of 2 cm^3/min H_2 (99.999%, AGA) and 48 cm^3/min He (9.996 %, AGA) yielding a total flow of 50 cm^3/min (4 vol-% H_2). The heating was started at ~ 25 °C (ramp rate 10 °C/min) and continued until ~800 °C.

2.4. In situ ETEM studies

Nucleation of Co nanoparticles and growth of SWNTs on ALD-$Co_xMg_{1-x}O$ were studied *in situ* using an aberration corrected FEI Titan 80-300FEG TEM operated at 300 kV.[4, 11, 17] The powders supported on bare Au TEM grid was heated up to 700 ^oC prior to introducing CO to grow carbon nanotubes. The maximum attainable pressure of CO in the ETEM chamber is ~10 mbar.

2.5. Growth of carbon nanotubes

A CCR1000 (Linkam) micro-reactor was applied to grow carbon nanotubes using CO as the carbon source.[4, 10, 14] About 20 mg catalyst powder was loaded into the sample holder and heated to 600 ^oC in the protection of Ar. After being stabilized at 600 ^oC, CO with a flow rate of 50 cm^3/min was introduced and the growth lasted for about 15 min. After growth, the CO flow was switched off and the system was cooled down in Ar.

2.6. Characterizations of carbon nanotubes

The as-grown carbon nanotubes were characterized by a Horiba Jobin-Yvon Labram300 Raman spectrometer. An excitation wavelength of 633 nm was used for the Raman measurements. TEM characterization was carried out using an aberration-corrected JEOL-2200FS FEG TEM/STEM operated at 80 kV. To purify the carbon nanotubes, the catalysts were removed by hydrochloric acid and the residual carbon nanotubes were rinsed with H_2O. After dispersing in a sodium cholate (NaC) aqueous solution and centrifugation, the carbon nanotube dispersions were characterized by UV-vis-NIR (Perkin Elmer, Lambda 950) absorption spectroscopy and photoluminescence excitation (PLE, Horiba Jobin-Yvon NanoLog-4) spectroscopy.

3. Results and discussion

3.1. Growth of carbon nanotubes on ALD-$Co_xMg_{1-x}O$ catalyst

The concentration of Co in ALD-$Co_xMg_{1-x}O$ determined by XPS is about 5%. Figure 1 depicts the XRD pattern of the ALD-$Co_xMg_{1-x}O$ catalyst. A prominent peak appears at 42.8° and relatively weak peaks occur at 36.9°, 62.2°, 74.5° and 78.5°, matching respectively with the (200), (111), (220), (311) and (222) planes for MgO. The XRD results suggest that the Co was dissolved in the MgO lattice forming a $Co_xMg_{1-x}O$ solid solution. Similar to the impregnation-prepared $Co_xMg_{1-x}O$ (1000),[4] the ALD-$Co_xMg_{1-x}O$ can also grow SWNTs at a relatively low temperature. As indicated by the presence of the radial breathing modes (RBMs) in the Raman spectrum of the product after growth at 600 °C (Supporting Information Figure S1). The high intensity ratio between G to D mode indicates that the SWNT purity/quality is high. The structures of the SWNTs were further confirmed by the TEM characterizations (Figure 1b). Clearly, high-quality SWNTs were produced despite the CVD growth temperature is not very high.

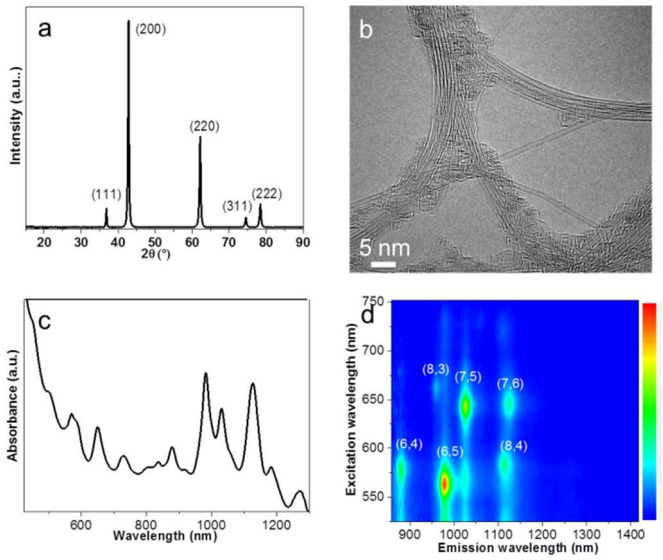

Figure 1 (a) XRD pattern of the ALD-$Co_xMg_{1-x}O$ catalyst. (b) A typical TEM image of purified SWNTs grown at 600 °C on ALD-$Co_xMg_{1-x}O$ catalyst. (c) UV-vis-NIR optical absorption spectrum of the SWNT dispersion. (d) Contour plots of normalized PLE intensities under the various excitation energies for the SWNT dispersion.

The SWNT chirality distribution was evaluated by absorption spectroscopy and photoluminescence spectroscopy. Figure 1c and 1d present respectively the absorption spectrum and the PLE map of SWNTs dispersed in NaC aqueous solution. In agreement with TEM characterization results, the product contains mainly small-diameter SWNTs. A preference to (6,5) and (7,5) tubes was observed in both the absorption spectrum and the PLE map. However, compared to the SWNTs grown on impregnation-prepared $Co_xMg_{1-x}O$(1000) under identical conditions (see Figure 5d in reference 4), the chirality distribution of SWNTs grown on the ALD-$Co_xMg_{1-x}O$ catalyst is relatively wide and the selectivity to (6,5) tubes is not high.

3.2. Growth mechanisms of SWNTs on ALD-$Co_xMg_{1-x}O$ catalyst

To understand the SWNT growth mechanisms and clarify the reasons for the chirality distribution differences of SWNTs grown on different solid solutions, *in situ* ETEM was applied to study the growth of carbon nanotubes on ALD-$Co_xMg_{1-x}O$. Prior to introducing CO, no Co nanoparticles were

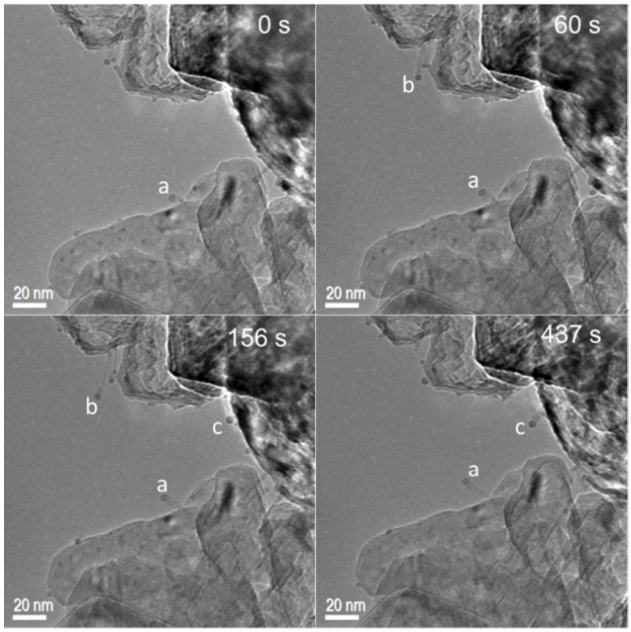

Figure 2 TEM image sequence taken from Movie S1, with time intervals displayed, showing that SWNTs grown on ALD-$Co_xMg_{1-x}O$ by "tip growth" mode.

observed on the surface of the catalyst (Supporting Information Figure S2). Growth of carbon nanotubes on the Co nanoparticles formed upon CO reduction at moderate temperature was observed (Supplementary Movie S1). Here, we note that, due to the low pressure condition in the ETEM chamber, the diameters of nanotubes are much larger than those of SWNTs grown by ambient pressure CVD.[4, 18] The time-series images (Figure 2) and the movie displaying the tube elongation process (tubes marked by a, b and c) clearly show that the SWNTs grow on ALD-$Co_xMg_{1-x}O$ by "tip growth" mode,[19-21] different from the "base growth" mode of SWNTs grown on $Co_xMg_{1-x}O(1000)$.[4] The different SWNT growth modes are supposed to be correlated with the different chirality distributions of SWNTs.

During SWNT nucleation and growth, the catalyst nanoparticle is supposed to act as a template,[22-24] as also verified by previous experimental work.[25-26] For example, by tuning the catalyst composition, i.e. the equilibrium shape of the catalytic nanoparticles, Chiang *et al.*[25] reported the growth of SWNTs with tuned chirality distribution. Upon exposing Fe nanoparticles to He/H_2O, Harutyunyan *et al.*[26] demonstrated pronounced faceting feature of Fe nanoparticles, leading to the preferential growth of metallic carbon nanotubes. The equilibrium shape of a supported nanoparticle is expressed by the Wulff-Kaischew theorem.[27-29] Certain crystal planes are preferred over others to minimize the surface energy, giving the equilibrium shape of a nanoparticle. Co nanoparticles formed upon ALD-$Co_xMg_{1-x}O$ reduction catalyze the growth of SWNTs via "tip growth" mode,[19-21] suggesting weak interactions between Co nanoparticles and underlying MgO support. While in the case of $Co_xMg_{1-x}O(1000)$, CO reduction leads to the formation of epitaxial metallic Co nanoparticles[4] (see also Supporting Information Figure S3). Owing to the epitaxial relationships with the MgO support, the reduced Co nanoparticles have extremely strong metal-support interactions[18] and catalyze the growth of SWNTs via "base growth" mode.[4, 9] The epitaxial strain acts against wetting so that it leads to a thickening of the nanoparticles, i.e. the nanoparticles have shapes with the ratio of height to length increasing with

the increasing lattice mismatch.[27-28] Therefore, the shape of the epitaxial Co nanoparticles differs from the near equilibrium Wulff shape that are adopted by Co nanoparticles formed by reducing ALD-$Co_xMg_{1-x}O$. Apparently the difference in shape and structure of Co nanoparticles leads to the growth of SWNTs with different chirality distribution. In general, the epitaxial Co nanoparticles adopt a uniform crystal structure with a well-defined orientation, thus facilitate growing SWNTs with a narrow chirality distribution.

3.3. Growth of carbon nanotubes on the $Co_xMg_{1-x}O(T)$ catalysts

As we discussed above, the impregnation prepared $Co_xMg_{1-x}O(1000)$ catalyst is suitable for synthesizing SWNTs with a high chiral-selectivity. To further elucidate the correlations between the catalyst performances and the catalyst preparation parameters, a series of impregnation-prepared $Co_xMg_{1-x}O(T)$ catalysts calcinated at different temperatures was applied for growing carbon nanotubes. Figure 3a shows the Raman spectra of carbon nanotubes grown on 4 different $Co_xMg_{1-x}O(T)$ catalysts

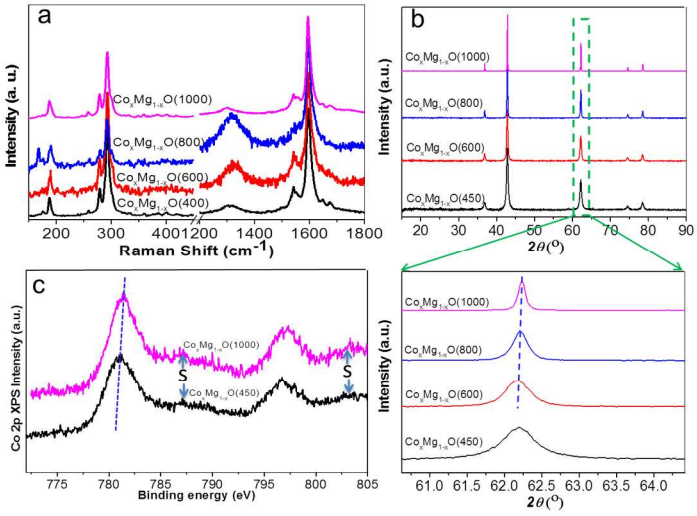

Figure 3 (a) Raman spectra of carbon nanotubes grown on 4 different $Co_xMg_{1-x}O$ catalysts calcinated at different temperatures. (b) XRD patterns of the 4 above-mentioned $Co_xMg_{1-x}O$ catalysts. Zoom in image shows the differences of the solid solutions upon calcination at different temperatures. (c) Comparison of Co 2p XPS spectra in $Co_xMg_{1-x}O(450)$ and $Co_xMg_{1-x}O(1000)$.

at 600 ^{o}C. The growth of SWNTs was observed on all the catalysts, as evidenced from the presence of RBMs in all the Raman spectra. However, only $Co_xMg_{1-x}O$(1000) yielded high quality/purity SWNTs, verified by the highest intensity ratio between G to D mode. The Raman spectra of SWNTs grown on $Co_xMg_{1-x}O$(800) and $Co_xMg_{1-x}O$(600) show relatively low G mode intensity and high D mode intensity, indicating the presence of large amount of carbonaceous impurities. Surprisingly, $Co_xMg_{1-x}O$(450) catalyzed the growth of SWNTs with higher quality/purity than the $Co_xMg_{1-x}O$(800) or $Co_xMg_{1-x}O$(600) did.

XRD characterization was performed for the 4 catalysts and their respective patterns are shown in Figure 3b. With the increased calcination temperature, the XRD peaks sharpen and the full width at half maximums of the diffraction peaks decrease, suggesting that the catalyst becomes more crystalline. The XRD patterns do not have a significant difference in comparison with that of pure MgO (JCPDS card no. 45-0946) or CoO (JCPDS card no. 48-1719) phase, indicating that there are no other Co species, like Co_3O_4 (JCPDS card no. 43-1003) in the catalysts. The 2θ peak positions show a slight shift towards higher values as the calcination temperature increases. This is because the relative concentrations of oxidic components of Co^{2+} differ from each other in the catalysts due to the different diffusion of Co^{2+} in MgO.[2, 30] At higher annealing temperature, the diffusion coefficient for Co^{2+} is larger, resulting in a deeper penetration of Co^{2+} in the MgO. This claim is also verified by the XPS characterization results. Satellite peaks corresponding to Co^{2+} were observed in both spectra of Co 2p shown in Figure 3c, the binding energy of Co $2p_{3/2}$ shifts upwards from 780.8 eV for $Co_xMg_{1-x}O$(450) to 781.3 eV for $Co_xMg_{1-x}O$(1000) catalyst, indicating that Co^{2+} in $Co_xMg_{1-x}O$(450) catalyst looks like CoO whereas Co^{2+} in $Co_xMg_{1-x}O$(1000) catalyst looks more like an ideal homogeneous solid solution. There are several components of oxidic Co^{2+} in solid solutions.[2, 31-32] One is the unreacted CoO particles located on the MgO surface. The fraction of CoO can be easily reduced, catalyzing the growth of MWNTs due to their large size and weak interactions with the oxide support. As verified in many

previous CoO-MgO systems,[6, 32] low temperature growth can only lead to the formation of MWNTs. Another component of the Co^{2+} is located on the subsurface layer within the MgO lattice. Such fraction of Co^{2+} is readily reduced at relatively low temperature and accounts for the growth of small diameter SWNTs at 400 °C.[4] The third fraction of the Co^{2+} is located a bit deeper than the subsurface layer within the MgO lattice and can also be reduced with increasing reduction temperature (denoted as near-subsurface Co^{2+}). The remaining fraction of Co^{2+} is located deep in the MgO lattice and is very difficult to reduce.

It has previously been shown that isolated CoO nanoparticles can hardly be observed on the surface of the raw $Co_xMg_{1-x}O(1000)$ catalyst,[4] suggesting that Co^{2+} ions exist mainly inside the MgO matrix. Upon CO reduction at 600 °C, the subsurface and near-subsurface Co^{2+} ions are readily reduced and

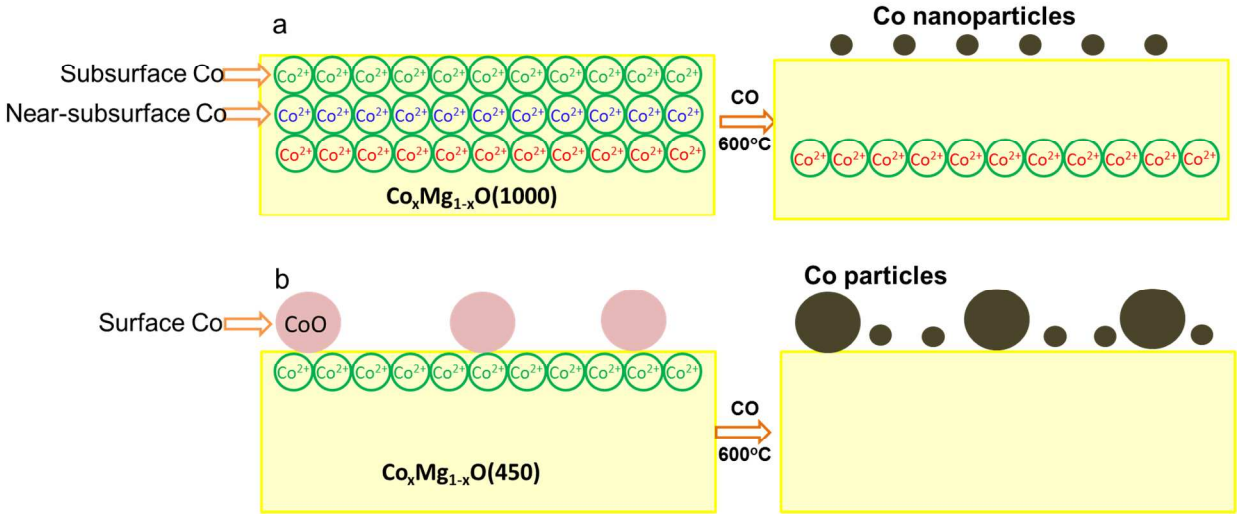

Figure 4 Schematic illustration of Co^{2+} reduction and formation of Co nanoparticles upon reducing of (a) $Co_xMg_{1-x}O(1000)$ and (b) $Co_xMg_{1-x}O(450)$.

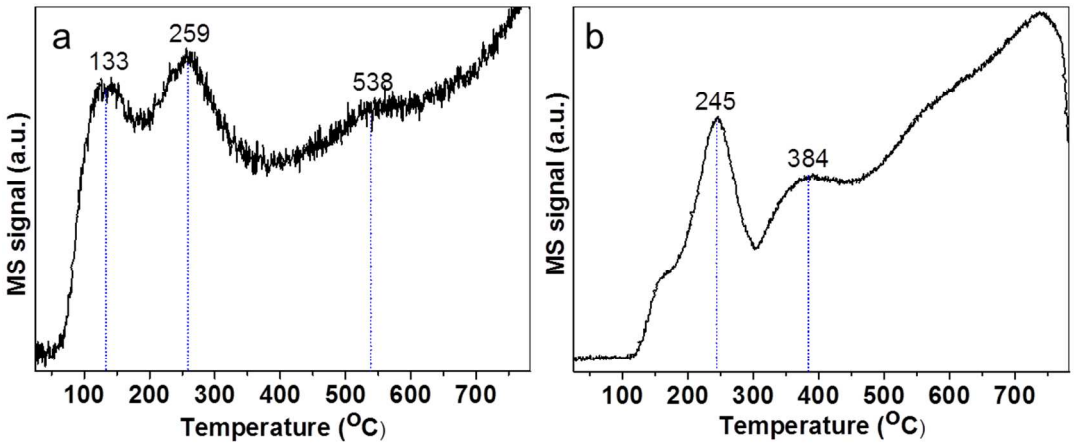

Figure 5 H_2-TPR profile of (a) $Co_xMg_{1-x}O(1000)$ and (b) $Co_xMg_{1-x}O(450)$. The formation of H_2O was monitored by mass spectrometry to follow reduction by H_2.

form small Co nanoparticles (Figure 4a), as observed by our *in situ* ETEM studies (Supporting Information Figure S3).[4] The reduction of near-subsurface Co^{2+} ions is mainly corresponding to the reduction peak of 538 °C in the H_2-TPR profile of $Co_xMg_{1-x}O(1000)$ (Figure 5a). SWNTs were also observed to grow on $Co_xMg_{1-x}O(1000)$ at 400 °C,[4] indicating Co^{2+} ions can be reduced to form small nanoparticles below 400 °C. The low temperature reduction of subsurface Co^{2+} ions is thus corresponding to the peak around 259 °C in its H_2-TPR profile. Interestingly, there is a low temperature H_2O formation peak at ~133 °C, which is probably due to the reduction of subsurface oxygen[33-34] in the $Co_xMg_{1-x}O(1000)$ catalyst. The presence of subsurface oxygen favors the reduction of the metal ions in the catalyst.[34]

In the case of $Co_xMg_{1-x}O(450)$ catalyst, CoO exists as both isolated CoO particles on the MgO surface and subsurface Co^{2+} ions. During the CVD growth process, both the surface CoO particles and subsurface Co^{2+} can be reduced and activated (Figure 4b). Although SWNTs can grow on Co nanoparticles extracted from reducing subsurface Co^{2+}, MWNTs grown on large Co particles from the reduction of surface CoO particles were frequently observed (Supporting Information Figure S4), as

also indicated by the dark black color of the final product. The assumption is further confirmed by the H_2-TPR profile of $Co_xMg_{1-x}O(450)$ (Figure 5b). The peak at 245 ^oC and 384 ^oC can be assigned as the reduction of large surface CoO nanoparticles and subsurface Co^{2+} ions in the $Co_xMg_{1-x}O(450)$ catalyst. While for $Co_xMg_{1-x}O(600)$, there is only one main reduction peak at 338 ^oC (Supporting Information Figure S5), corresponding to the reduction of large CoO nanoparticles on the surface, accounting for the low SWNT purity of the product grown at 600 ^oC. The depletion of subsurface and near-subsurface Co^{2+} ions in $Co_xMg_{1-x}O(600)$ is due to the relatively high calcination temperature. It is noted that the concentration of subsurface and near-subsurface Co^{2+} ions in $Co_xMg_{1-x}O(1000)$ is also high, resulting from the diffusion of surface CoO at such a calcination temperature. The Co^{2+} diffusion and depletion mechanisms were further verified by the facts that almost no carbon deposition was observed on the $Co_xMg_{1-x}O(1200)$ catalyst at 600 ^oC using CO as carbon source.

To understand how the catalyst reducibility affects the SWNT chirality distribution, PLE

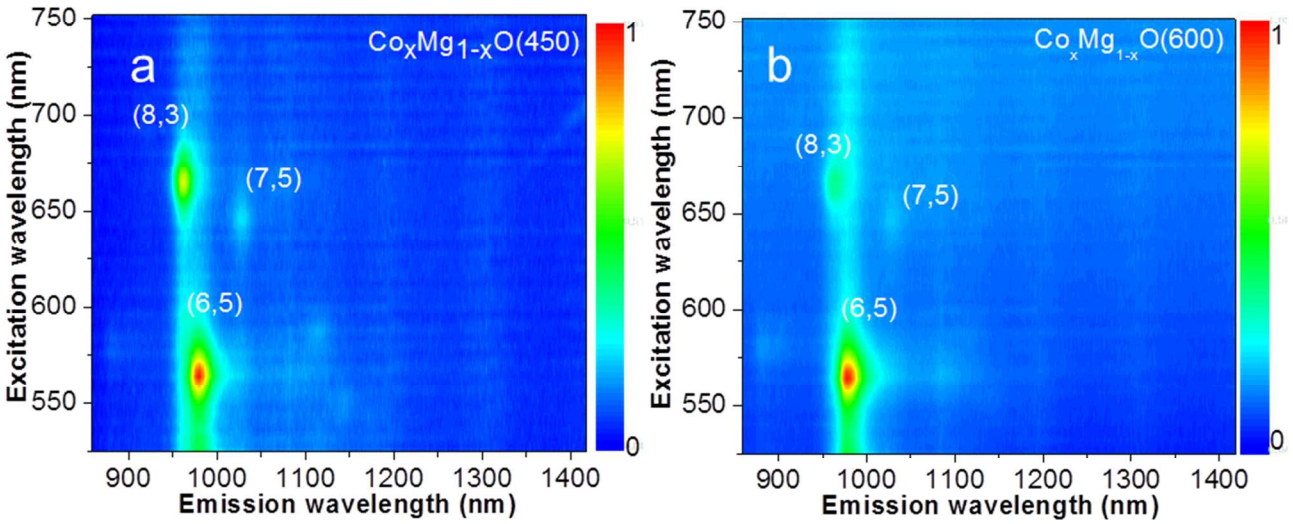

Figure 6 Contour plots of normalized photoluminescence emission intensities under the various excitation energies for SWNTs grown on (a) $Co_xMg_{1-x}O(450)$ and (b) $Co_xMg_{1-x}O(600)$ at 600 ^oC.

measurements were conducted on the dispersions of SWNTs grown on different $Co_xMg_{1-x}O(T)$ catalysts. Figure 6a and 6b show the PLE maps of SWNTs grown on $Co_xMg_{1-x}O(450)$ and $Co_xMg_{1-x}O(600)$, respectively. Despite the fact that the SWNT purities of the products are inferior to tubes grown on $Co_xMg_{1-x}O(1000)$, the SWNT chirality distributions are comparable to that of SWNTs grown on the $Co_xMg_{1-x}O(1000)$ catalyst.[4] A predominant growth of (6,5) SWNTs was observed in both samples. Except for (6,5), (8,3) and (7,5) tubes, the concentrations of other tube species are negligible. The results show that the $Co_xMg_{1-x}O$ catalysts calcinated at lower temperatures can also afford the growth of SWNTs with a narrow chirality distribution. If the formation of large CoO particles on the catalyst surface can be avoided by improving the impregnation process, it is feasible to obtain high-purity SWNTs on solid solutions calcinated at low temperatures.

4. Conclusions

Chiral-selective growth of SWNTs was achieved on a newly developed ALD-$Co_xMg_{1-x}O$ catalyst. Compared with the chirality distribution of SWNTs grown on impregnation prepared $Co_xMg_{1-x}O(T)$ catalysts, the chirality distribution of SWNTs grown on ALD-$Co_xMg_{1-x}O$ is a bit wider and shows relatively low chirality selectivity. *In situ* ETEM studies revealed a "tip-growth" mode of SWNTs grown on the ALD-$Co_xMg_{1-x}O$ catalyst, suggesting weak interactions between reduced Co nanoparticles and the MgO support, thus a lack of structural control over the Co nanoparticles. The findings indicate the epitaxy-related "base growth" is of great importance in growing SWNTs with a high chiral selectivity on $Co_xMg_{1-x}O(T)$ catalysts. Finally, the roles of calcination in the catalytic performances of impregnation-prepared $Co_xMg_{1-x}O$ catalysts were also investigated systematically. Our work presented in this paper helps understand the growth mechanisms of SWNTs, especially demonstrates a potential of tuning SWNT chirality distribution by regulating the strengths of metal-support interactions.

Acknowledgements

This work was funded by the CNB-E Project in Aalto University through the Multidisciplinary Institute of Digitalization and Energy (MIDE) program. Financial support by the NorTEMnet project (NordForsk), RFBR-13-02-01354 and RAS research programs are acknowledged. The A.P. Møller and Chastine Mc-Kinney Møller Foundation is gratefully acknowledged for their contribution towards the establishment of the Center for Electron Nanoscopy in the Technical University of Denmark. The authors acknowledge the Laboratory of Inorganic Chemistry of Aalto University for access to XRD and Mr. Matti Lehtimäki for his assistance with the measurements.

Supplementary data: 1. Extensive figures of the characterization results of catalyst and carbon nanotubes. 2. *In situ* ETEM movie showing the growth of carbon nanotubes on ALD-$Co_xMg_{1-x}O$ catalyst by "tip growth" mode. The frame rate is about 5 times faster than the real carbon nanotube growth rate.

TOCs:

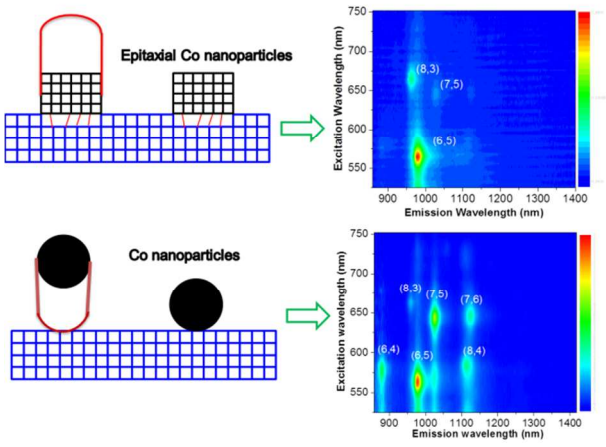

Single-walled carbon nanotube grown by base-growth mode (top) and tip-growth mode (bottom) show a striking contrast in chirality distributions.

References

1 Y. H. Hu, E. Ruckenstein, *Catal. Rev.*, 2002, **44**, 423-453.

2 H. Y. Wang, E. Ruckenstein, *Carbon*, 2002, **40**, 1911-1917.

3 P. Chen, H. B. Zhang, G. D. Lin, Q. Hong, K. R. Tsai, *Carbon*, 1997, **35**, 1495-1501.

4 M. He, H. Jiang, B. Liu, P. V. Fedotov, A. I. Chernov, E. D. Obraztsova, F. Cavalca, J. B. Wagner, T. W. Hansen, I. V. Anoshkin, E. A. Obraztsova, A. V. Belkin, E. Sairanen, A. G. Nasibulin, J. Lehtonen, E. I. Kauppinen, *Sci. Rep.*, 2013, **3**, 1460.

5 E. Flahaut, A. Peigney, C. Laurent, A. Rousset, *J. Mater. Chem.*, 2000, **10**, 249-252.

6 L. Qingwen, Y. Hao, C. Yan, Z. Jin, L. Zhongfan, *J. Mater. Chem.*, 2002, **12**, 1179-1183.

7 E. Flahaut, R. Bacsa, A. Peigney, C. Laurent, *Chem. Commun.*, 2003, 1442.

8 G. Lolli, L. Zhang, L. Balzano, N. Sakulchaicharoen, Y. Tan, D. E. Resasco, *J. Phys. Chem. B*, 2006, **110**, 2108-2115.

9 J. Gavillet, A. Loiseau, C. Journet, F. Willaime, F. Ducastelle, J. C. Charlier, *Phys. Rev. Lett.*, 2001, **87**.

10 M. He, A. I. Chernov, P. V. Fedotov, E. D. Obraztsova, J. Sainio, E. Rikkinen, H. Jiang, Z. Zhu, Y. Tian, E. I. Kauppinen, M. Niemela, A. O. Krause, *J. Am. Chem. Soc.*, 2010, **132**, 13994-13996.

11 M. He, B. Liu, A. I. Chernov, E. D. Obraztsova, I. Kauppi, H. Jiang, I. Anoshkin, F. Cavalca, T. W. Hansen, J. B. Wagner, A. G. Nasibulin, E. I. Kauppinen, J. Linnekoski, M. Niemela□, J. Lehtonen, *Chem. Mater.*, 2012, **24**, 1796-1801.

12 M. He, A. I. Chernov, E. D. Obraztsova, H. Jiang, E. I. Kauppinen, J. Lehtonen, *Carbon*, 2013, **52**, 590–594.

13 L. B. Backman, A. Rautiainen, A. O. I. Krause, M. Lindblad, *Catal. Today*, 1998, **43**, 11-19.

14 M. He, A. I. Chernov, P. V. Fedotov, E. D. Obraztsova, E. Rikkinen, Z. Zhu, J. Sainio, H. Jiang, A. G. Nasibulin, E. I. Kauppinen, M. Niemela, A. O. Krause, *Chem. Commun.*, 2011, **47**, 1219-1221.

15 M. He, S. Vasala, H. Jiang, M. Karppinen, E. I. Kauppinen, M. Niemela, J. Lehtonen, *Carbon*, 2012, **50**, 4750-4754.

16 S. Ardizzone, C. L. Bianchi, M. Fadoni, B. Vercelli, *Appl. Surf. Sci.*, 1997, **119**, 253-259.

17 T. W. Hansen, J. B. Wagner, R. E. Dunin-Borkowski, *Mater. Sci. Technol.*, 2010, **26**, 1338-1344.

18 B. Wang, L. Wei, L. Yao, L. J. Li, Y. Yang, Y. Chen, *J. Phys. Chem. C*, 2007, **111**, 14612-14616.

19 L. X. Zheng, M. J. O'Connell, S. K. Doorn, X. Z. Liao, Y. H. Zhao, E. A. Akhadov, M. A. Hoffbauer, B. J. Roop, Q. X. Jia, R. C. Dye, D. E. Peterson, S. M. Huang, J. Liu, Y. T. Zhu, *Nat. Mater.*, 2004, **3**, 673-676.

20 J. C. Charlier, H. Amara, P. Lambin, *ACS Nano*, 2007, **1**, 202-207.

21 H. J. Dai, *Top. Appl. Phys.*, 2001, **80**, 29-53.

22 S. Reich, L. Li, J. Robertson, *Chem. Phys. Lett.*, 2006, **421**, 469-472.

23 M. Diarra, A. Zappelli, H. Amara, F. Ducastelle, C. Bichara, *Phys. Rev. Lett.*, 2012, **109**, 185501.

24 D. A. Gomez-Gualdron, J. Zhao, P. B. Balbuena, *J. Chem. Phys.*, 2011, **134**, 014705.

25 W.-H. Chiang, R. Mohan Sankaran, *Nat. Mater.*, 2009, **8**, 882-886.

26 A. R. Harutyunyan, G. Chen, T. M. Paronyan, E. M. Pigos, O. A. Kuznetsov, K. Hewaparakrama, S. M. Kim, D. Zakharov, E. A. Stach, G. U. Sumanasekera, *Science*, 2009, **326**, 116-120.

27 C. R. Henry, *Prog. Surf. Sci.*, 2005, **80**, 92-116.

28 P. Mullen, R. Kern, *Surf. Sci.*, 2000, **457**, 229-253.

29 S. Valeri, S. Benedetti, P. Luches, *J Phys-Condens Mat*, 2007, **19**, 225002.

30 B. J. Wuensch, T. Vasilos, *J. Chem. Phys.*, 1962, **36**, 2917-2922.

31 F. Arena, F. Frusteri, A. Parmaliana, N. Giordano, *React. Kinet. Catal. Lett.*, 1990, **42**, 121-126.

32 B. Wang, Y. Yang, L.-J. Li, Y. Chen, *J. Mater. Sci.*, 2009, **44**, 3285-3295.

33 F. Esch, S. Fabris, L. Zhou, T. Montini, C. Africh, P. Fornasiero, G. Comelli, R. Rosei, *Science*, 2005, **309**, 752-755.

34 X. W. Liu, K. B. Zhou, L. Wang, B. Y. Wang, Y. D. Li, *J. Am. Chem. Soc.*, 2009, **131**, 3140-3141.

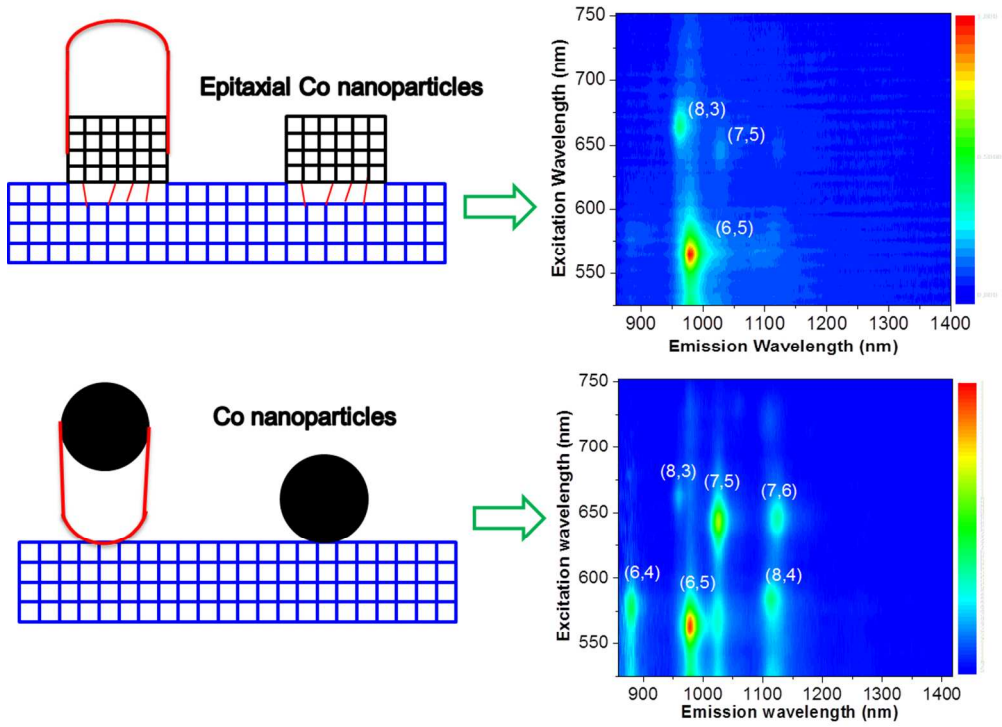

Single-walled carbon nanotube grown by base-growth mode (top) and tip-growth mode (bottom) show a striking contrast in chirality distributions.
315x238mm (96 x 96 DPI)